Non-Foster Loaded Parasitic Array for Broadband Steerable Patterns

Minu M. Jacob, *Student Member, IEEE*, Jiang Long, *Student Member, IEEE*, and Daniel F. Sievenpiper, *Fellow, IEEE*

***Abstract*—Parasitic arrays can generate steerable patterns using tunable reactive loads at the parasitic elements to provide the required phase for the scattered radiation. However, the radiation that is coupled to the parasitic elements and reflected by the attached loads has a frequency dependent phase delay, leading to a beam/null squint effect and a limited instantaneous squint-free bandwidth. In this paper, we introduce a technique for eliminating this frequency dependence using non-Foster parasitic loads, whose reflection phase has a positive phase dispersion slope that can cancel the negative phase dispersion slope associated with propagation delays. Further, by tuning the non-Foster load, we can tune the total scattered phase to achieve steerable patterns. Tunable non-Foster impedances can be designed using transistor-based negative impedance convertor (NIC) circuits. A two element parasitic array was designed for the frequencies of operation of discrete device NICs. Non-Foster impedances required for obtaining broadband or squint-free nulls at different azimuth angles were calculated using array theory and simulations. An NIC that generated the non-Foster impedance for a broadside broadband null was fabricated and attached to the parasitic antenna. Simulation and measurement results showed broadband uniform nulls from 180–350 MHz, providing about twice the null bandwidth of a passive parasitic load. Null steering across some angles of the azimuth was restricted by the stability constraints of the NIC while being tuned. With a judicious design of the parasitic antenna and the NIC, we can achieve broader bandwidths and steerable patterns with non-Foster parasitic arrays.**

***Index Terms*—Negative impedance convertor, non-foster circuit, parasitic array.**

I. Introduction

ADVANCEMENTS in mobile communications have led to a need for broadband, low cost, light weight antenna array systems with electronically steerable beams and nulls. Phased array antennas with true time delay beamforming can provide broadband (squint-free) beam or null steering, but at the cost of a complex feed network and complicated RF signal processing circuitry [1]. On the other hand, steerable parasitic arrays such as electronically steerable parasitic array radiator (ESPAR) antennas involve only a single fed element along with one or more parasitic elements attached to tunable impedances, and can provide low cost beam or null steering [2]–[4]. However, parasitic arrays have a limited instantaneous squint-free bandwidth, typically 10–15%.

In parasitic arrays, the radiated field from the driven element couples to the parasitic elements, gets reflected from the attached load impedances, and is re-radiated back into free space where it adds to the direct radiation from the driven element to form a beam or null pattern [5]. The phase delays incurred over the coupling, reflection and re-radiation process is frequency dependent, leading to a beam or null squint effect beyond a small bandwidth of operation. The dispersive phase delay associated with propagation through physical distances or reflection from Foster impedances (passive components of +L and/or +C) has a negative slope with frequency. To cancel this inherent phase dispersion and achieve broadband performance, we require a dispersive element that has an equivalent positive phase dispersion slope. This can be obtained with negative delay elements or alternatively, with non-Foster impedances.

Non-Foster impedances are components such as negative inductors and/or negative capacitors whose reactance has a negative slope with frequency [6]. They are realized using active, transistor based negative impedance convertor (NIC) or negative impedance inverter (NII) circuits [7], [8]. We have reported different applications of these circuits, as active matching networks to overcome the bandwidth limitations of small antennas [9], and in superluminal waveguides for broadband leaky-wave antennas [10], [11]. Further, the negative slope of the reactance of non-Foster impedances translates to a positive slope in their reflection phase, which can be estimated as an equivalent negative delay. In this paper, we utilize the "negative delay" characteristics of non-Foster elements to broaden the bandwidth of parasitic arrays by attaching non-Foster loads (active components of –L and/or -C) at the parasitic elements to provide a positive-slope reflection phase that cancels the negative-slope propagation phase to eliminate phase dispersion. We can also achieve beam or null steering by tuning the non-Foster load impedances to provide the required phase for a null or beam in a particular direction.

This paper introduces basic array theory for a two element parasitic array to identify the non-Foster circuit required for broadband beams or nulls. For a small array, the beam will be very broad, but the null will be much narrower. It is much easier to see and quantitatively define the null position (a sharp dip) than the beam position. For this array, the "squint-free bandwidth" or equivalently, the "null bandwidth" is the bandwidth within which all frequencies have the same squint-free null angle. A two element parasitic array is designed for the operation frequencies appropriate for discrete device NICs, and array theory is used to calculate non-Foster impedances

Manuscript received August 02, 2013; revised May 02, 2014; accepted July 10, 2014. Date of publication October 08, 2014; date of current version November 25, 2014. This work was supported by DARPA and the AFRL under contract FA8650-07-D-1114-0004.

The authors are with the University of California, San Diego, La Jolla, CA 92093 USA (e-mail: mmjacob@ucsd.edu; jilong@ucsd.edu; dsievenpiper @eng.ucsd.edu).

Color versions of one or more of the figures in this paper are available online at http://ieeexplore.ieee.org.

Digital Object Identifier 10.1109/TAP.2014.2361903

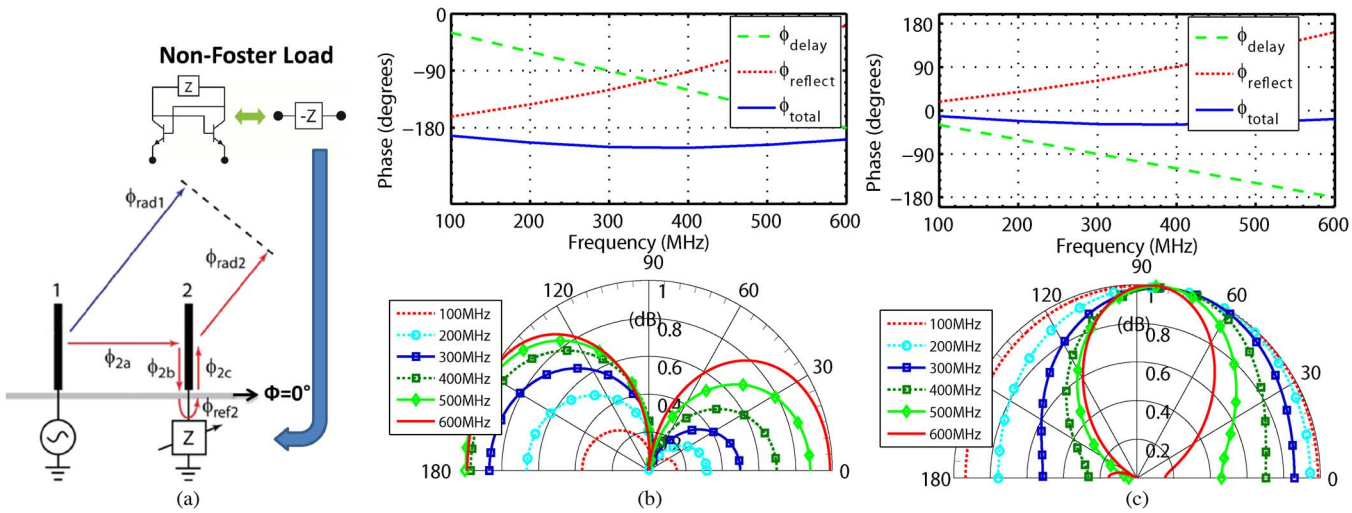

Fig. 1. (a) A two element non-Foster loaded parasitic array model used to calculate the total phase dispersion due to propagation and reflection. (b) Cancellation of the delay phase with the reflection phase from a parallel $-\mathrm{L}||-\mathrm{C}$ load to obtain a net phase of 180° at $\Phi = 90°$ and a resultant broadband null from 100–600 MHz. (c) Cancellation of the delay phase with the reflection phase from a series –L-C load to obtain a net phase of 0° at $\Phi = 90°$ and a resultant broadband beam from 100–600 MHz.

required for broadband nulls at different azimuth angles. EM/circuit co-simulation has been used to calculate radiation patterns for different non-Foster parasitic loads and these have been compared with those of passive parasitic loads to show that non-Foster parasitic loads achieve broader squint-free bandwidths for almost all azimuth angles. Stability conditions are analyzed for NICs attached to parasitic antennas, and a stable NIC is fabricated and attached to the parasitic antenna. Measurements for a broadband, broadside null have been performed and compared to co-simulation patterns, demonstrating an almost 2:1 instantaneous null bandwidth. This can be compared to one of the broadest reported bandwidths for a conventional parasitic array [12] which contains 24 parasitic elements that are switched on or off to produce two separate partially overlapping beam steering modes achieving a total simulated 2:1 gain bandwidth. However, the instantaneous bandwidth during a single mode of operation is less than 2:1. In contrast, the non-Foster parasitic array has a measured instantaneous 2:1 bandwidth with just one parasitic element. However, the tunability of this particular non-Foster array is limited by the stability constraints of the NIC. Design considerations to improve stability of the non-Foster parasitic array over a broad tuning range have been presented.

II. Parasitic Array Design and Fabrication

A simple two element parasitic array loaded with a non-Foster impedance has been modeled as shown in Fig. 1(a). The elements are assumed to be infinitesimally small with a 25 cm separation between them. The array factor patterns for two non-Foster loads, namely a parallel –L-C impedance of $-12\ \mathrm{nH}||-5\ \mathrm{pF}$ and a series –L-C impedance of -12 nH–5 pF have been shown in Fig. 1(b) and (c) respectively. The coupling phase or delay phase Φ_{delay} from the driven element to the parasitic element has a negative slope with frequency (as seen in the phase plots of Fig. 1(b) and (c)). The reflection phase Φ_{reflect} from the non-Foster load will have a positive slope with frequency (as seen in the phase plots of Fig. 1(b) and (c)). The array factor patterns are obtained after adding the propagation delay phase and the reflection phase from the attached load. We see that when the non-Foster load is a parallel –L-C impedance of $-12\ \mathrm{nH}||-5\ \mathrm{pF}$, the reflection phase from it cancels the delay induced phase dispersion to provide a net phase Φ_{total} of around -180 degrees from 100–600 MHz at $\Phi = 90°$ along the azimuth, leading to a broadband null (Fig. 1(b)). When the non-Foster load is a series –L-C impedance of -12 nH–5 pF, the reflection phase from it cancels the delay induced phase dispersion to provide a net phase Φ_{total} of around 0 degrees from 100–600 MHz at $\Phi = 90°$, leading to a broadband beam (Fig. 1(c)). This simplified model provides the same squint-free patterns across a 6:1 bandwidth. However in reality, the matching and coupling characteristics of the antennas, unwanted scattering effects, non-uniform radiation patterns and non-ideal non-Foster loads reduce the achievable bandwidth.

In a parasitic array, the driven antenna should be well matched to accept incoming signals and should also have a high enough gain to be able to radiate to the parasitic elements. The distance between the driven element and the parasitic elements should be optimized to have sufficient coupling between them while reducing unwanted scattering. The design of the antennas should also take into consideration the practical performance limits of NICs. Since discrete device NICs can only generate broadband, high quality factor non-Foster impedances for frequencies less than 400 MHz, a prototype of a two element parasitic array was designed for those frequencies. At those low frequencies, an antenna array that could achieve good matching and coupling with uniform patterns across a broad bandwidth was difficult to design due to the following tradeoffs: large antennas are needed for broadband match; however, large antennas have non-uniform patterns within the required range of frequencies. Small antennas provide uniform patterns, reduced spacing and less unwanted scattering, but do not have the required matching or gain. It will also be shown later that the parasitic antenna's impedance should satisfy the stability conditions of the NIC.

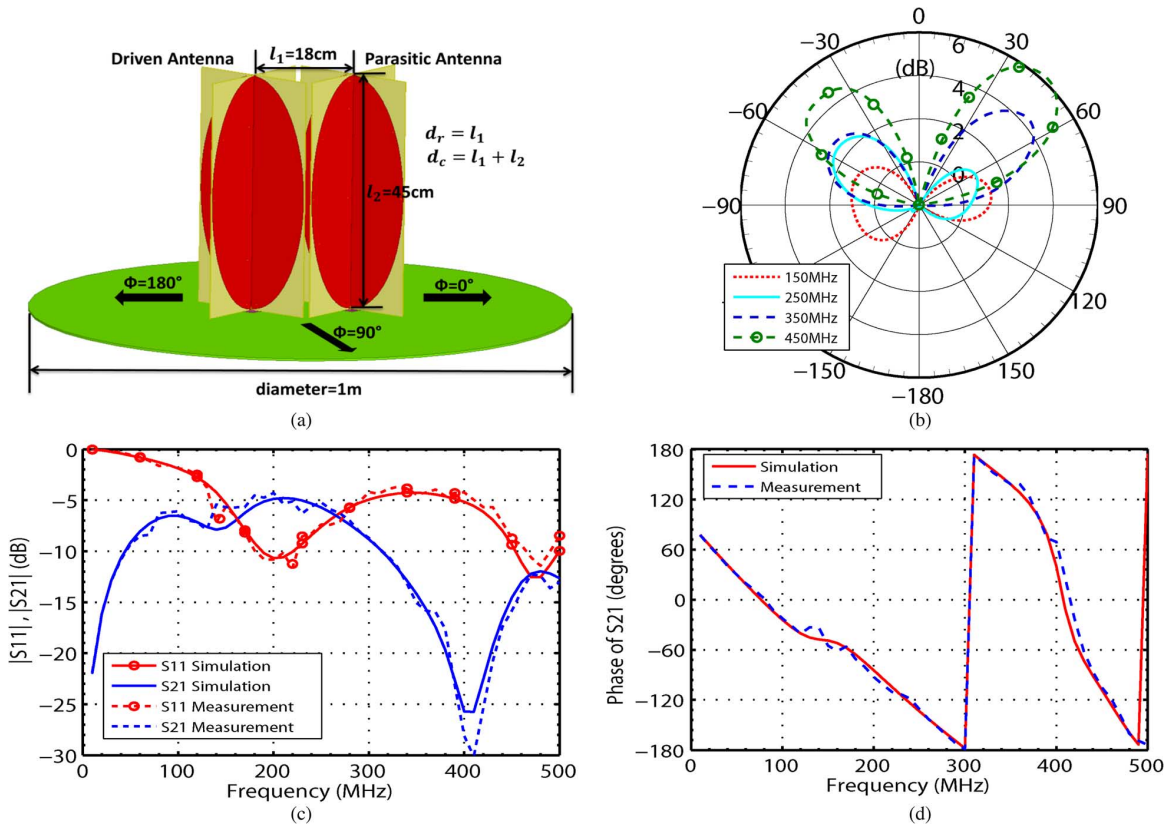

Fig. 2. (a) Simulated two element array. (b) Simulated elevation patterns of a single antenna. (c) Simulated and measured $\mathrm{S}_{11}(\mathrm{dB})$ and $\mathrm{S}_{21}(\mathrm{dB})$. (d) Simulated and measured phase of S_{21}.

Optimized simulations in Ansoft HFSS yielded a bulb-shaped monopole array design that provided the required matching and coupling characteristics across the broadest possible bandwidth (150 MHz–350 MHz) with uniform patterns in those frequencies. The monopole had a height of 45 cm, width of 24 cm, and the distance between the driven and parasitic element was 18 cm. The antennas were mounted on a circular aluminum ground plane of diameter 1 m (Fig. 2(a)). The elevation patterns of a single bulb-monopole antenna mounted on the ground plane are simulated and shown in Fig. 2(b). Due to the finite ground plane, we see that the angle of maximum radiation is not horizontal for high frequencies. This can be corrected using a ground plane with a conducting sleeve as described in [13]. The elevated main beams at frequencies above 350 MHz limit the highest frequency that can be observed in the squint-free null bandwidths, as can be seen in the next section. The azimuth patterns of a single bulb-monopole antenna are omnidirectional for these frequencies. The parasitic array design was fabricated and tested and found to agree well with simulations. The simulated and measured matching (S_{11}) and coupling (S_{21}) characteristics of the passive array are shown in Fig. 2(c) and (d). Ideally, S_{11} should be as small as possible, indicating a good impedance match, and S_{21} should be close to 1, indicating good coupling between the two antennas. But due to the tradeoffs mentioned before, a good match and high coupling could not be achieved across the entire bandwidth. However, the measured pattern results of the non-Foster array follow the theoretical array theory (that assumes ideal S_{21}) sufficiently well to indicate that the performance of the two element array falls within acceptable limits.

III. Non-Foster Parasitic Arrays—Theory and Bandwidth Improvement

A. Array Theory to Identify Non-Foster Impedances for Null/Beam Tuning

The fabricated 2 element antenna array can be modeled using the schematic shown in Fig. 1(a), where antenna 1 is the driven element and antenna 2 is the parasitic element. The array factor can then be derived as

$$\mathrm{AF} = 1 + |S_{21}| \times e^{j(\phi_{\mathrm{coupling}} + \phi_{\mathrm{reflection}} + \phi_{\mathrm{radiation}})} \tag{1}$$

where,

$$\phi_{\mathrm{coupling}} = \phi_{2a} + \phi_{2b} + \phi_{2c} = \frac{\pi}{2} - k \times d_c = \angle S_{21} \tag{2}$$

$$\phi_{\mathrm{radiation}} = \phi_{\mathrm{rad2}} = k \times d_r \times \cos(\phi) \tag{3}$$

$$\phi_{\mathrm{reflection}} = \phi_{\mathrm{ref2}}. \tag{4}$$

Here, Φ_{coupling} is the coupling phase from antenna 1 to antenna 2, and is the total sum of the propagation phase Φ_{2a} along the distance of separation, along with the propagation phase $\Phi_{2b} + \Phi_{2c}$ through the parasitic antenna (Fig. 1(a)). The coupling phase is equivalent to $(\pi/2) - k \times d_c$ where the added phase of $\pi/2$ is due to the capacitive coupling of the monopole array. The variable k is the wavenumber, and d_c is the coupling distance which equals the distance of separation plus the antenna height. The term $\Phi_{\mathrm{radiation}}$ is the radiation phase which denotes the difference in the far-field radiated phase between the

driven element and the parasitic element for an azimuth angle Φ where Φ has the values denoted in Fig. 2(a). It is equivalent to $k\ d_r \cos(\Phi)$, where d_r is equal to the distance of separation. The term $\Phi_{\text{reflection}}$ is the reflection phase Φ_{ref2} from the load attached to the parasitic antenna.

For easier analysis, we assume that the coupling loss $|S_{21}|$ is negligible. In order to get broadband nulls along an azimuth angle Φ, the sum of the coupling phase, reflection phase and radiation phase should equal π radians. This means that the reflection phase should be

$$\phi_{\text{reflection}} = \pi - \phi_{\text{coupling}} - \phi_{\text{radiation}} \tag{5}$$

which implies,

$$\phi_{\text{reflection}} = \pi - \frac{\pi}{2} + k \times d_c - k \times d_r \times \cos(\phi). \tag{6}$$

In other words,

$$\phi_{\text{reflection}} = \pi - \angle S_{21} - k \times d_r \times \cos(\phi). \tag{7}$$

From (6), we observe that in order to achieve 180° of total phase across a broad bandwidth, the reflection phase will need to have a positive slope with frequency (since d_c will always be greater than d_r). This reflection phase can be obtained with non-Foster impedances (-L,-C).

B. Tunable Nulls with Ideal $-\mathrm{L}||-\mathrm{C}$

The measured S_{21} data of the parasitic array is used to calculate the required non-Foster reflection phase. To identify the –L,-C combination needed for providing the required phase, we first calculate the reflection phase needed to produce a null along say, $\Phi = 180°$ (in the direction away from the parasitic antenna) using (7). This phase has a positive slope as can be seen from Fig. 3. When we simulate the reflection phases of –L, -C, series –L-C and parallel –L-C, we see that a parallel –L-C can give us the required reflection phase in the entire operation region of the parasitic array (150–350 MHz), as seen in Fig. 3. The reflection phase of the series –L-C can also approximate the required phase, but only for a limited low frequency region. By choosing the correct value of –L and –C, we can dictate the slope and resonance frequency of the reflection phase. Even if the phase of S21 is not exactly linear with respect to frequency, we can tune the values of –L and –C to get the required phase slope.

Fig. 4 shows the reflection phase required for squint-free nulls along the angles of $\Phi = 0°$, $\Phi = 90°$ and $\Phi = 180°$, calculated using (7). The directions of these angles with respect to the driven and parasitic antennas are shown in Fig. 2(a). As the null angle increases, the reflection phase slope becomes steeper. With non-Foster impedances of $-\mathrm{L}||-\mathrm{C}$, we can achieve good approximations of the theoretical reflection phase curves. The –L, –C values required for each of the 3 null directions are also given in Fig. 4.

Using Ansoft HFSS and Ansoft Designer, we were able to dynamically link the parasitic array EM model to a circuit model of $-\mathrm{L}|-\mathrm{C}$ to get radiation patterns for different values of –L and –C in the region of operation of the parasitic array (150–350 MHz). The azimuth patterns obtained from co-simulations are

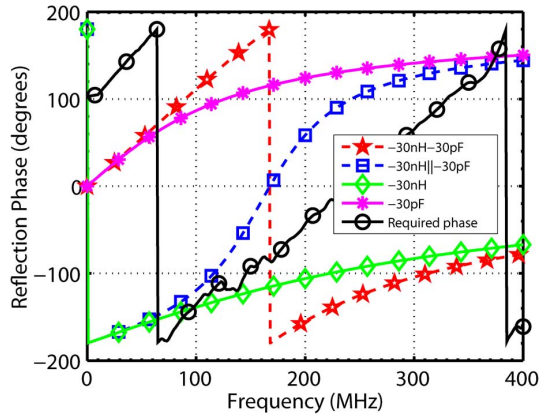

Fig. 3. Required non-Foster reflection phase for getting a squint-free null along 180° for the fabricated array, and the reflection phases of ideal –L,-C components.

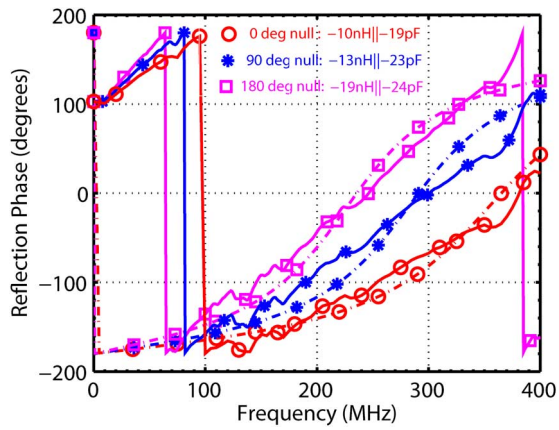

Fig. 4. Required non-Foster reflection phases calculated using array theory for a broadband null at 0°, 90° and 180° (solid lines). Reflection phases of $-\mathrm{L}||-\mathrm{C}$ impedances (dotted lines) that approximate the theoretical phase curves.

shown in Fig. 5. For the 0° null case (Fig. 5(a)), we obtained broadband nulls when the parasitic antenna was shorted (-1 nH load), similar to the case of a reflector antenna. For the 90° null (Fig. 5(b)) and 180° null (Fig. 5(c)), the values of –L and –C obtained from Fig. 4 had to be modified slightly in order to broaden the bandwidth. This might be due to scattering effects that were unaccounted for in the simple mathematical phase calculation. The lowest and highest frequencies providing squint free nulls are shown for each of the 3 null directions, along with some intermediate frequencies. From these, we see that we can achieve the broadest bandwidth for the 0° null. As the null angle increases, the bandwidth decreases. However, null tuning can be achieved across all azimuth angles, with broader bandwidths than those obtained with traditional Foster parasitic arrays.

C. Squint-Free Bandwidth Improvement

We will verify the improvement in squint-free bandwidth by studying the maximum achievable bandwidth with both Foster and non-Foster loads for different null angles. Simulations were done using the designed two element bulb-monopole array and various Foster loads (+L, +C combinations) and non-Foster loads (-L, -C combinations). The parasitic loads that gave the

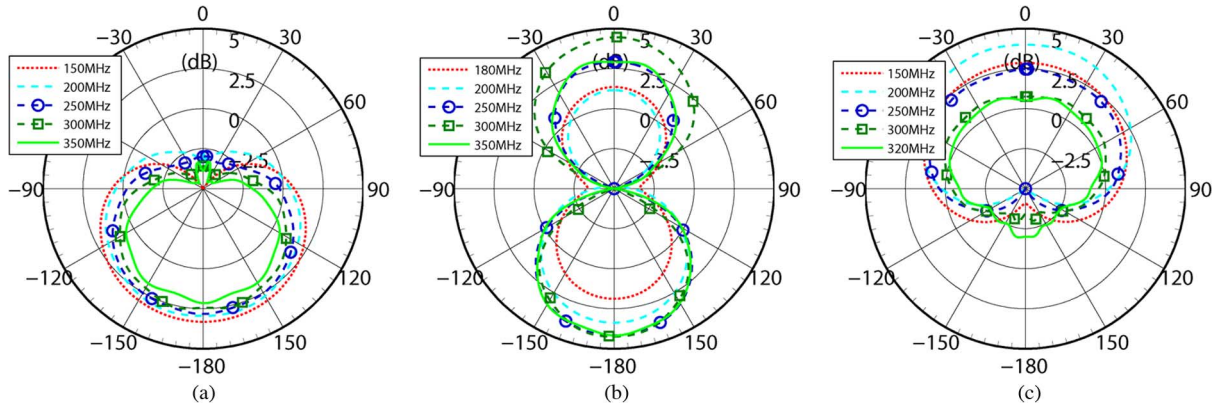

Fig. 5. Broadband nulls obtained from ideal –L-C co-simulations with antenna array. (a) Null at 0° obtained with −1 nH. (b) Null at 90° obtained with −15 nH|| −23 pF. (c) Null at 180° obtained with −19 nH|| − 30 pF.

TABLE I
SQUINTY FREE NULL FREQUENCIES FOR NON-FOSTER AND FOSTER PARASITIC LOADS

Null Position (degree)	Non-Foster Load and the Squint-Free Frequencies	Foster Load and the Squint-Free Frequencies
0°	Short :150-350 MHz	Short :150-350 MHz
45°	-13nH||-17pF :170-350 MHz	31 pF :190-350 MHz
90°	-15nH||-23pF :180-350 MHz	30nH+5pF :220-300 MHz
135°	-16nH||-28pF :180-330 MHz	10nH+6.5pF :210-200 MHz
180°	-19nH||-30pF :150-320 MHz	Open :170-220 MHz

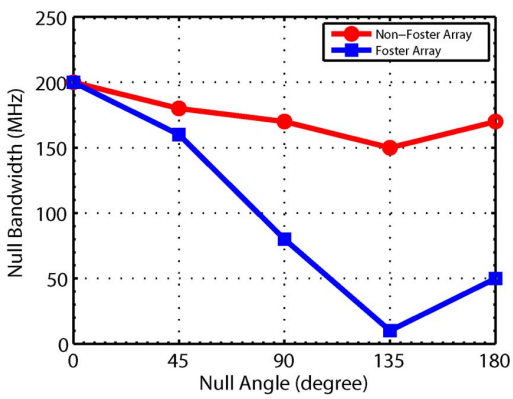

Fig. 6. Bandwidth of squint-free nulls for different null positions obtained with the non-Foster and Foster parasitic loads in Table I.

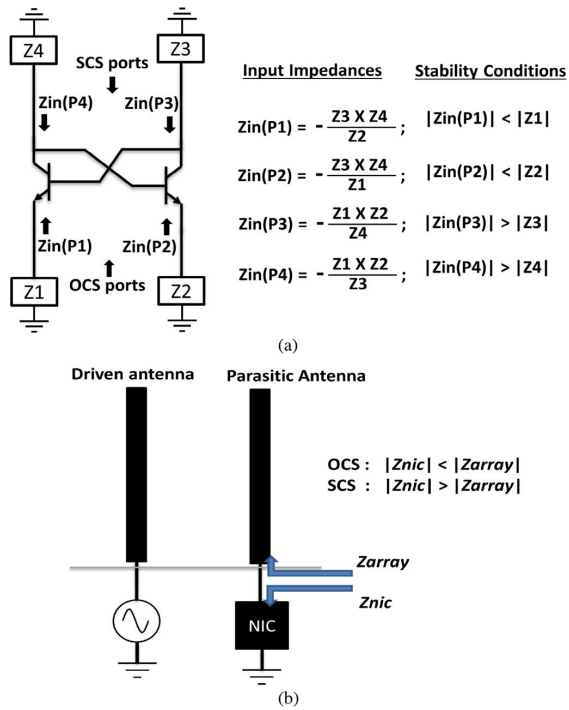

Fig. 7. (a) General topology of a negative impedance convertor (NIC) circuit and the input impedances seen into each of the four ports. (b) OCS and SCS stability conditions of the NIC attached to the parasitic antenna.

broadest squint-free bandwidth for nulls at 0°, 45°, 90°, 135° and 180° are shown in Table I. While assessing the bandwidth for each null angle, we allowed a ± 20° variation around the null angle considered for both the Foster and non-Foster cases. We also optimized for parasitic loads that resulted in patterns where the null gain was at least 3 dB lower than the beam gain for all frequencies in the squint-free bandwidth. In general, it is more difficult to obtain squint-free nulls than it is to obtain squint-free beams, due to the formation of small backlobes or sidelobes that could change the null position, while the beam position remains the same. The results are summarized in Fig. 6.

We see that for the 0° null angle, the parasitic element acts like a reflector and so we can achieve the broadest possible bandwidth with a short. As the null is tuned away from the parasitic element, the maximum achievable bandwidth decreases for both Foster and non-Foster loads. Nevertheless, we see that non-Foster elements can provide a larger bandwidth of squint-free nulls compared to Foster elements for almost all azimuth angles.

The non-Foster impedances in Table I can be achieved using discrete device NICs for the operation frequencies of the designed parasitic array. However, the stability constraints of NICs pose a considerable challenge, as shown in the next section.

IV. NIC DESIGN AND STABILITY CONSIDERATIONS

Non-Foster impedances can be implemented using NIC circuits or NII circuits [7], [14]. These circuits have a general cross coupled transistor topology (Fig. 7(a)). The input impedance seen at each of the 4 ports, and the conditions for stability at

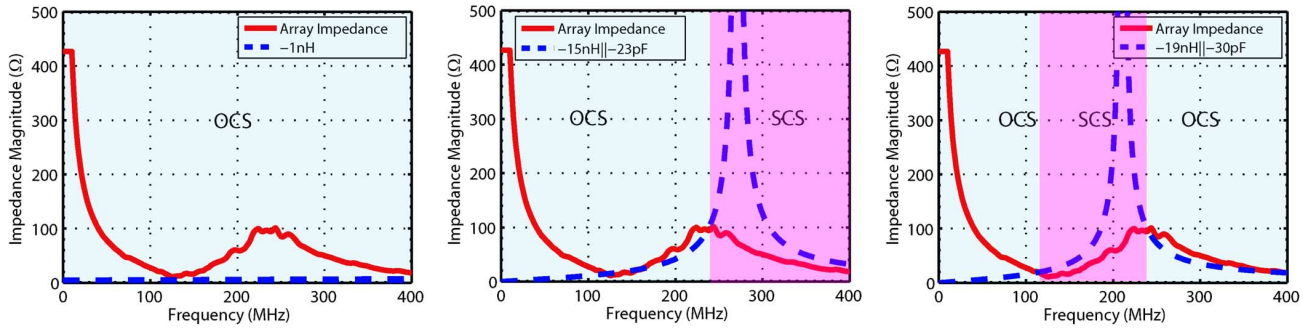

Fig. 8. Required stability conditions of the non-Foster impedances when loaded to the antenna array for the (a) 0° null using −1 nH, (b) 90° null using −15 nH||−23 pF, and (c) 180° null using −19 nH|| − 30 pF.

each of those ports are also shown in Fig. 7(a). A primary challenge in the design of NICs is to maintain stability while generating broadband, low loss non-Foster reactances. A number of theories have been suggested to analyze the stability constraints of NICs [15]–[18].

A. Stability Analysis

In general, if Z_{NIC} is the required input impedance of the NIC and Z_{load} is the load impedance to be attached at the input, the two stable conditions of the NIC are as follows:

1) If $|Z_{load}| > |Z_{NIC}|$, then the NIC should be implemented in its open circuit stable (OCS) configuration with its input at the transistor's emitter.
2) If $|Z_{load}| < |Z_{NIC}|$, then the NIC should be implemented in its short circuit stable (SCS) configuration with its input at the transistor's base/collector.

Fig. 7(b) shows the stability criteria for our two element parasitic array with an NIC attached to the parasitic antenna. Z_{array} is the impedance seen by the NIC looking into the parasitic antenna and Z_{NIC} is the input impedance of the NIC. Fig. 8 displays the magnitude of Z_{array}, along with the magnitude of the NIC impedance Z_{NIC} for the different –L,-C values taken from Fig. 5 for different null angles.

For the 0° null angle using a -1 nH load, $|Z_{NIC}|$ is always less than $|Z_{array}|$ and so the NIC will be stable in its OCS configuration (Fig. 8(a)).

For the 90° null angle using a -15 nH$||-23$ pF load, $|Z_{NIC}|$ is less than $|Z_{array}|$ up to 260 MHz (OCS condition), and $|Z_{NIC}|$ is greater than $|Z_{array}|$ above 260 MHz (SCS condition). This means that the NIC has to have the OCS configuration to be stable under 260 MHz, while simultaneously requiring the SCS configuration to be stable above 260 MHz (Fig. 8(b)).

For the 180° null angle using a -19 nH$|| - 30$ pF load, the NIC has to have the OCS configuration up to 120 MHz, SCS configuration from 120 MHz–240 MHz, and OCS configuration again from 240 MHz–400 MHz (Fig. 8(c)).

This implies that for the NIC to be stable across the entire bandwidth of operation, the NIC impedance should be either completely above or completely below the antenna array impedance for all frequencies of interest. For the monopole array considered here with a parallel –L-C load, the NIC has to have the OCS configuration for low frequency stability (since $-\mathrm{L}||-\mathrm{C}$ is a short at low frequencies while the monopole is an open at low frequencies). Further, in order to maintain OCS stability across the entire bandwidth of operation, we have to reduce the quality factor Q of the NIC impedance so that its peak impedance during its resonance is less than the antenna impedance at that frequency. This means that we will have to sacrifice the nullforming performance of the parasitic array. Even with those conditions, it is still not possible to achieve the 180° null angle with the NIC since the Q of the NIC would have to be far too low in order to satisfy OCS stability conditions around 100 MHz. Therefore, we see that the tunability and nullforming capabilities of the parasitic array are restricted by the stability conditions of the non-Foster impedance.

B. Circuit Design and Fabrication

From the stability analysis, we know that the NIC circuit has to have an OCS configuration, with its input at one of the transistor emitters. Since we require a parallel $-\mathrm{L}||-\mathrm{C}$ impedance, we can either use a NIC configuration to negate the impedance of a positive parallel $+\mathrm{L}||+\mathrm{C}$, or we can use a NII configuration to negate the admittance of a positive series +L+C. We chose to use the NII configuration, since it would help us transition into a tunable circuit (using a tunable varactor in the NII circuit will give us a tunable –L impedance) [19].

The NIC circuit for the 0° null angle is trivial since we can get the same result with a short circuit. The NIC circuit for the 180° null angle has too many stability constraints with this particular antenna impedance for it to be physically realizable. Therefore we chose to implement the circuit needed for a 90° null angle (NIC impedance of -15 nH$|| - 23$ pF). In order for the NIC to be OCS stable with the antenna, we will have to reduce the NIC's quality factor Q, and slightly push the resonance of the NIC to lower frequencies so that the NIC's peak impedance is not much higher than the antenna's peak impedance.

Fig. 9(a) shows the schematic of an NII circuit that gives us an impedance equivalent to $-\mathrm{L}||-\mathrm{C}$. The impedance of the NII circuit seen looking into the emitter of BJT1 is inversely proportional to the emitter load of BJT2 and directly proportional to the loads at the two base-collector junctions as shown in the schematic of Fig. 7(a). Since the emitter load of BJT2 is a series LC impedance of Ind1 and Cap1, the impedance of the NII will take the form of a parallel $-\mathrm{L}||-\mathrm{C}$ impedance as required. The loads at the two base-collector junctions, namely $\mathrm{R9}+(\mathrm{Cap2}||\mathrm{R8})$ and $\mathrm{R10}+\mathrm{Ind2}$ have been chosen to optimize

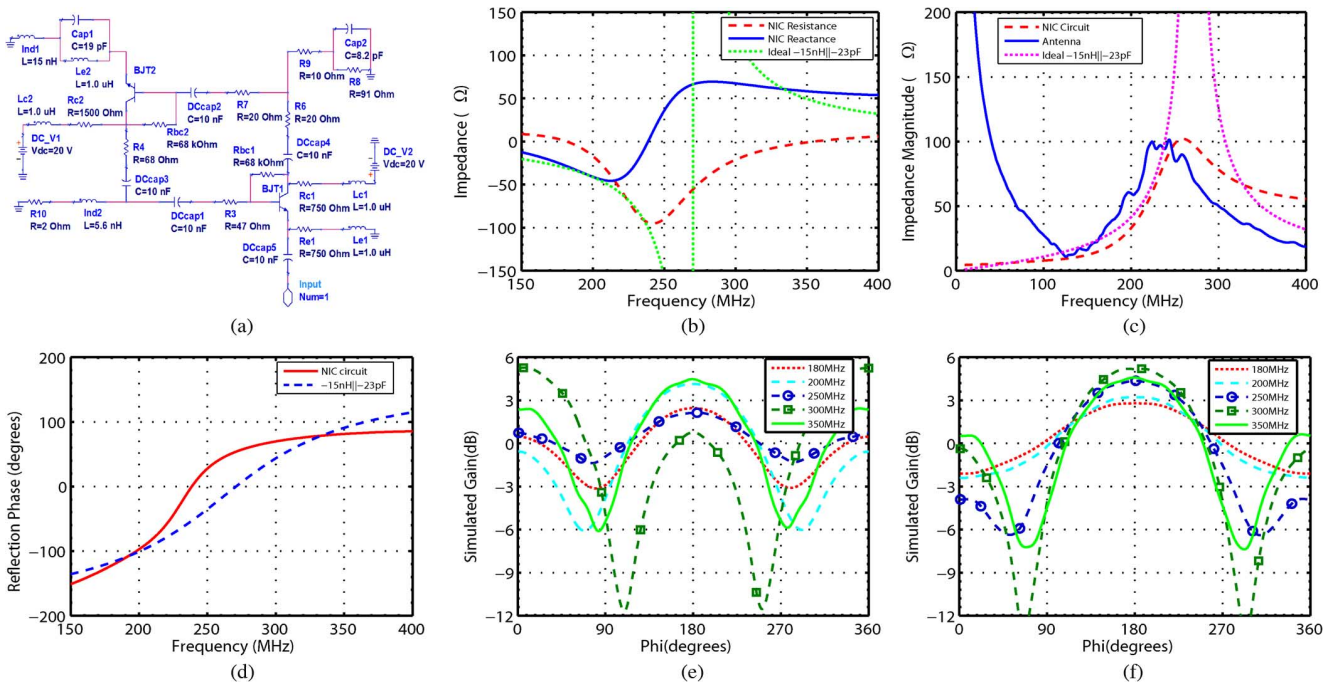

Fig. 9. (a) NII circuit design for getting a 90° null and (b) the simulated real and imaginary non-Foster impedance of the circuit compared to the ideal impedance required. (c) The reduced quality factor of the circuit impedance to achieve stability with the antenna impedance. (d) Reflection phase of the NII circuit compared to the ideal required reflection phase. (e) Radiation patterns obtained from co-simulations with the NII circuit and array. (f) Radiation patterns obtained from co-simulations after changing the NII circuit impedance.

the quality factor Q of the circuit. Resistors R3, R4, R6 and R7 have been used to stabilize the circuit. The circuit layout was simulated in Ansoft HFSS and the device models were attached and optimized in Agilent ADS to provide a high enough Q for the circuit that it would produce broadband 90° null patterns, yet a low enough Q that it would be stable with the antenna. The resistance and reactance of the simulated NII (taking into account all the component and layout parasitics) is shown in Fig. 9(b).

Fig. 9(c) shows the simulated impedance magnitude of the stable NII circuit along with the antenna impedance and the ideal $-\mathrm{L}||-\mathrm{C}$ impedance. The circuit was tuned to the edge of stability where the circuit impedance magnitude has just crossed over the antenna impedance magnitude, as seen in Fig. 9(c). We see that the Q has been reduced and that the resonance has been slightly pushed to lower frequencies. Even though the NII impedance is still greater than the antenna impedance at higher frequencies, the gain of the NII is sufficiently less at those frequencies to prevent instability. However, this is the edge of stability and a slight shift of the resonance to higher frequencies causes instability.

In Fig. 9(d), the input reflection phase of the NII has been compared to the ideal required reflection phase from -15 nH$||-23$ pF. The greatest variation in phase from the ideal case is observed around 250 MHz, which corresponds to the resonant frequency of the NII (Fig. 9(b)). The impedance of the NII has been significantly damped at the resonant frequency to provide stability, leading to a phase variation around that frequency.

Fig. 9(e) shows the patterns obtained by dynamically linking the simulated circuit with the EM model of the antenna. Although the null angle is not as uniform as for the ideal $-\mathrm{L}||-\mathrm{C}$ case, it is still an improvement over the bandwidth and null-forming performance obtained from Foster loads. A broadband squint-free 90° null was obtained from 180–350 MHz.

To obtain steerable squint-free beams/nulls, we need tunable –L,-C impedances. These can be obtained with a tunable negative capacitor with an NIC and a varactor, and a tunable negative inductor with an NII and a varactor. With integrated circuit technology, we can design tunable NICs or NIIs that can provide high quality factor non-Foster impedances in the UHF frequencies [19]. It is also feasible to switch between fixed –L,-C impedances based on the beam/null angle required. In the NII schematic of Fig. 9(a), the main components affecting the impedance of the circuit are the inductor Ind1 and capacitor Cap1 at the emitter of BJT2. The capacitor Cap1 can be replaced by a varactor to enable tunability, resulting in a tunable –L at the input. The inductor Ind1 cannot be tuned in this NII configuration, so the –C value of this NII circuit cannot be tuned. We will get the best possible beam/null steering capabilities with two separate circuits for a negative inductor and negative capacitor, so that either can be individually tuned to provide the required reflection phase for any beam/null direction. With only a tunable varactor in place of the capacitor Cap1 in the NII circuit, we can only achieve certain null positions. When Cap1 is changed from 19 pF to 10 pF, we see from the co-simulation patterns that the null position moves from 90° to about 60° (Fig. 9(f)).

Due to the one port configuration of the NII, and the fact that it is stable only when attached to the antenna (equivalent to some RLC impedance), we could not get a de-embedded measurement of the NII. However, our simulation techniques have proven to be very reliable with other NIC designs and measurements [20], [11] and so we proceeded to pattern measurements with the parasitic array.

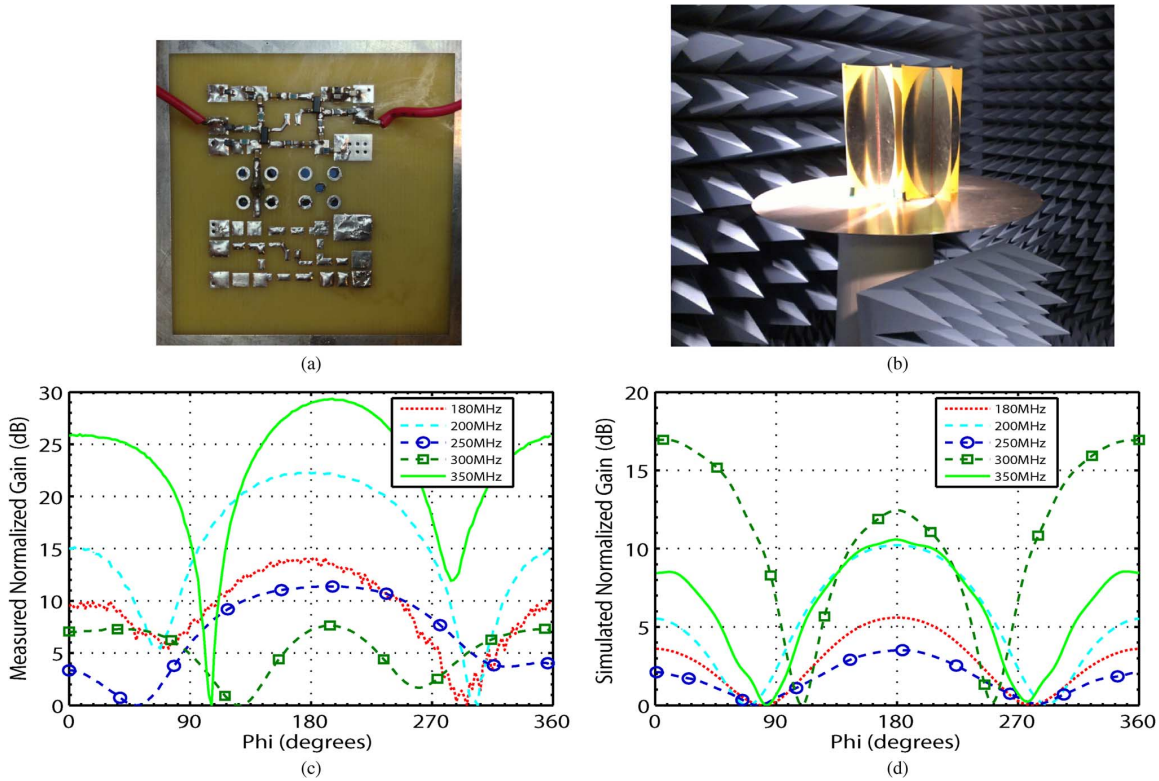

Fig. 10. (a) Fabricated NII circuit. (b) Measurement setup in an anechoic chamber. (c) Measured normalized gain patterns. (d) Co-simulated normalized gain patterns.

V. Squint-Free Pattern Measurements

The NII was fabricated and attached to the base of the parasitic antenna. We then supplied the required DC voltage to the NII circuit and attached the driven antenna to a spectrum analyzer so that any instability in the NII would be coupled from the parasitic antenna to the driven antenna and show up as peaks above the noise floor in the spectrum analyzer. We also tested our stability analysis by trying to push the $-\mathrm{L}||-\mathrm{C}$ resonance to slightly higher frequencies and found that it did indeed lead to instability.

After implementing the stable circuit shown in Fig. 10(a), we measured the parasitic array's patterns in an anechoic chamber as shown in Fig. 10(b). Although the chamber's dimensions were too small for accurate low frequency gain measurements, we did get sufficiently smooth patterns with null positions that agreed with simulations (Fig. 10(c)). The measurements were plotted after normalizing each frequency's pattern separately to its minimum measured gain value to get a null gain relative to beam gain for each frequency. The normalized gain values shown have not been calibrated for the path loss and the gain of the receiving horn antenna, and so the measurements are only indicative of the null positions and not the actual gain. The actual gain can be observed from the co-simulation patterns shown in Fig. 9(e). The co-simulation patterns have further been normalized and plotted in Fig. 10(d).

We see from the measurement patterns (Fig. 10(c)) and the co-simulation patterns (Fig. 10(d)), that the null positions for all frequencies from 180–350 MHz have less than a $\pm 30^\circ$ variation about 90° and 270°. The frequencies from 240–310 MHz show the biggest variation from the 90° null position compared to the co-simulation patterns, since that frequency region corresponds to the resonance region of the NII making it very sensitive to component variations in the circuit. Thus we see that the null forming performance of the NII is affected by the $-\mathrm{L}||-\mathrm{C}$ resonance of the NII and the stability constraints requiring the NII to have low Q and a lower resonant frequency. However, these measured results display a squint-free bandwidth that is more than a factor of 2 better than the bandwidth obtained with Foster parasitic loads. This non-Foster parasitic array was designed to demonstrate its squint-free nullforming capability, so gain analysis and optimization has not been done. Further studies can be done to improve the gain using better antenna and array designs. The nullforming capabilities in the resonant region of the circuit can also be improved using antenna designs that impose less stringent stability requirements on the non-Foster circuit. For a non-Foster parasitic array operating at higher frequencies, accurate gain measurements could be obtained to validate the simulated gain.

VI. Design Considerations for a Stable, Tunable, Broadband Non-Foster Parasitic Array

It was shown that the tunability of the parasitic array was restricted by the stability constraints of the NIC set by the impedance of the parasitic antenna. We will introduce an alternate approach to design a stable, broadband non-Foster parasitic array with tuning capabilities. First, it is important to choose an NIC that has similar impedance curves as the antenna array to prevent the NIC impedance from crossing over the antenna impedance in the frequencies of interest. This means that for a loop antenna array, we should choose a parallel –L-C (both have a parallel LC impedance magnitude), and for a dipole array, we should choose a series –L-C (both have

a series LC impedance magnitude). Then, we have to design the coupling distance dc such that the required non-Foster phase can be obtained with the NIC. For example, assuming we have a dipole array (requiring a series –L-C), we have to design the array such that the coupling distance dc (distance of separation+ antenna height) leads to a theoretical non-Foster reflection phase that can be achieved by a series –L-C. If the coupling distance dc is too large, then the required non-Foster reflection phase will undergo a second resonance (from $-180°$ to $+180°$), which cannot be achieved by a series –L-C.

Once the total coupling distance dc is known, the antenna height or size can be chosen such that it has sufficient gain and matching, and the antenna separation can be chosen to have sufficient coupling. The antenna impedance can further be optimized to provide broadband stable conditions for the NIC.

This technique of using non-Foster circuit loads is especially suited for parasitic arrays with a few antenna elements so that the coupling between the elements is clearly defined and the required non-Foster reflection phase can be easily achieved with an NIC. For elements with more than one parasitic element, the coupling between the elements is defined by a coupling matrix, which can be used in the array factor equation to determine the required non-Foster reflection phase. Alternatively, optimization techniques mentioned in [2] and [21] can be used to find the reactive loads for multiple frequencies in a required broad bandwidth, and the calculated reactances will be found to follow a non-Foster reactance curve versus frequency.

Another important consideration in an active non-Foster circuit is the noise added by the circuit and the resulting SNR degradation. When the signal coupled to the parasitic element is reflected by the non-Foster circuit attached to the parasitic element, a frequency dependent noise generated by the circuit is added to the existing environmental noise in the signal. The noise performance of non-Foster parasitic arrays is beyond the scope of this paper, but we are currently studying noise characteristics of non-Foster circuits to analyze the possible tradeoffs between bandwidth improvement and SNR degradation.

VII. Conclusion

A novel technique has been introduced to eliminate beam/null squint arising from phase dispersion in parasitic arrays. Using non-Foster loaded parasitic elements, we can compensate for the propagation delay phase by introducing an equivalent negative delay associated with the reflection phase of non-Foster elements. An additional phase could also be imposed by the non-Foster elements to achieve a beam or null. Further, by tuning the non-Foster impedance, we could tune the angle of the beam/null. We have developed the theory of non-Foster parasitic arrays to show that a non-Foster reflection phase is required for a frequency-independent beam/null angle, and to identify the non-Foster impedance required for a particular beam/null angle. We have tested this theory with a two element monopole array and ideal –L, -C impedances. A non-Foster circuit designed to achieve squint-free null patterns has been fabricated, and measurements of squint-free radiation patterns have been compared with simulation results. Stability constraints of the NIC relating to the antenna impedance have been identified, and an approach to mitigate stability and tunability constraints has been suggested. We have also examined the bandwidth advantage of non-Foster parasitic arrays over Foster parasitic arrays. Our measurement results verify the theoretical analysis, and demonstrate scope for improvements. This prototype could be improved to include tunable –L and –C circuits to obtain reconfigurable squint-free patterns. A further study on the bandwidth-tunability-nullforming tradeoffs could be useful in developing an electronically tunable, broadband, low cost parasitic array without beam/null squint.

References

[1] I. Frigyes and A. J. Seeds, "Optically generated true-time delay in phased-array antennas," *IEEE Trans. Microw. Theory Tech.*, vol. 43, pp. 2378–2386, 1995.

[2] R. F. Harrington, "Reactively controlled directive arrays," *IEEE Trans. Antennas Propag.*, vol. 26, pp. 390–395, 1978.

[3] K. Gyoda and T. Ohira, "Design of electronically steerable passive array radiator (ESPAR) antennas," in *Proc. IEEE Antennas and Propagation Society Int. Symp.*, 2000, vol. 2, pp. 922–925.

[4] B. Alshami, H. Aboulnour, and M. Dib, "Design of a broadband ESPAR antenna," in *Proc. Mediterranean Microwave Symp.*, 2009, pp. 1–6.

[5] J. D. Kraus, *Antennas*, 2nd ed. New York, New York, USA: McGraw-Hill, 1988.

[6] R. M. Foster, "A reactance theorem," *Bell Syst. Tech. J.*, vol. 3, pp. 259–267, Apr. 1924.

[7] J. G. Linvill, "Transistor negative-impedance converters," in *Proc. IRE*, 1953, vol. 41, pp. 725–729.

[8] S. E. Sussman-Fort and R. M. Rudish, "Non-foster impedance matching of electrically-small antennas," *IEEE Trans. Antennas Propag.*, vol. 57, pp. 2230–2241, 2009.

[9] M. M. Jacob, L. Jiang, and D. F. Sievenpiper, "Broadband non-foster matching of an electrically small loop antenna," in *Proc. IEEE Antennas and Propagation Society Int. Symp.*, 2012, pp. 1–2.

[10] D. F. Sievenpiper, "Superluminal waveguides based on non-foster circuits for broadband leaky-wave antennas," *IEEE Antennas Wireless Propag. Lett.*, vol. 10, pp. 231–234, 2011.

[11] L. Jiang, M. Jacob, and D. F. Sievenpiper, "Electronically steerable antenna using superluminal waveguide and tunable negative capacitors," in *Proc. IEEE Antennas and Propagation Society Int. Symp.*, 2012, pp. 1–2.

[12] A. Sutinjo, M. Okoniewski, and R. H. Johnston, "An octave band switched parasitic beam-steering array," *IEEE Antennas Wireless Propag. Lett.*, vol. 6, pp. 211–214, 2007.

[13] R. Schlub and D. V. Thiel, "Switched parasitic antenna on a finite ground plane with conductive sleeve," *IEEE Trans. Antennas Propag.*, vol. 52, pp. 1343–1347, 2004.

[14] A. Larky, "Negative-impedance converters," *IRE Trans. Circuit Theory*, vol. 4, pp. 124–131, 1957.

[15] R. D. Middlebrook, "Null double injection and the extra element theorem," *IEEE Trans. Ed.*, vol. 32, pp. 167–180, 1989.

[16] M. Tian, V. Visvanathan, J. Hantgan, and K. Kundert, "Striving for small-signal stability," *IEEE Circuits Dev. Mag.*, vol. 17, pp. 31–41, 2001.

[17] S. D. Stearns, "Non-foster circuits and stability theory," in *Proc. IEEE Int. Symp. on Antennas and Propagation*, 2011, pp. 1942–1945.

[18] S. D. Stearns, "Incorrect stability criteria for non-foster circuits," in *Proc. IEEE Antennas and Propagation Society Int. Symp.*, 2012, pp. 1–2.

[19] C. R. White, J. W. May, and J. S. Colburn, "A variable negative-inductance integrated circuit at UHF frequencies," *IEEE Microw. Wireless Compon. Lett.*, vol. 22, pp. 35–37, 2012.

[20] D. Sievenpiper, M. Jacob, and J. Long, "Active electromagnetic structures, metamaterials, antennas," in *Proc. IEEE Int. Workshop on Antenna Technology*, 2012, pp. 289–292.

[21] T. Ohira and K. Iigusa, "Electronically steerable parasitic array radiator antenna," *Electron. Commun. Jpn. (Part II: Electron.)*, vol. 87, pp. 25–45, 2004.

Minu M. Jacob (S'11) received the B.S. degree from Amrita School of Engineering, Coimbatore, India, in 2009. She is currently working toward the Ph. D. degree at the University of California, San Diego, CA, USA.

Her current research interests include non-Foster circuits and their applications in antennas and metamaterials.

Jiang Long (S'11) received the B.S. and M.S. degrees from Zhejiang University, Hangzhou, China, in 2007 and 2010, respectively. He is currently working toward the Ph. D. degree at the University of California, San Diego, CA, USA.

His current research area is non-foster loaded artificial impedance surface metamaterials.

Daniel F. Sievenpiper (M'94–SM'04–F'09) received the B.S. and Ph.D. degrees in electrical engineering from the University of California, Los Angeles, CA, USA, in 1994 and 1999, respectively.

He is currently a Professor at the University of California, San Diego, where his research focuses on antennas and electromagnetic structures. Prior to 2010, he was the Director of the Applied Electromagnetics Laboratory, HRL Laboratories, Malibu, CA, USA, where his research included artificial impedance surfaces, conformal antennas, tunable and wearable antennas, and beam steering methods. He holds more than 70 issued patents and has been published in more than 60 technical publications.

Prof. Sievenpiper was awarded the URSI Issac Koga Gold Medal in 2008 and in 2009 he was named as a Fellow of the IEEE. Since 2010, he has served as an Associate Editor of the IEEE ANTENNAS AND WIRELESS PROPAGATION LETTERS. He currently serves as the Chair of the IEEE Antennas and Propagation Society Committee on New Technology Directions.